$BRAF^{V600E}$-Driven Lung Adenocarcinoma Requires Copper to Sustain Autophagic Signaling and Processing

Tiffany Tsang[1,2,3], Xingxing Gu[1,2], Caroline I. Davis[1,2,4], Jessica M. Posimo[1,2], Zoey A. Miller[1,2,5], and Donita C. Brady[1,3]

ABSTRACT

The transition metal copper (Cu) is an essential micronutrient required for development and proliferation, but the molecular mechanisms by which Cu contributes to these processes is not fully understood. Although traditionally studied as a static cofactor critical for the function of Cu-dependent enzymes, an expanding role for Cu is emerging to include its novel function as a dynamic mediator of signaling processes through the direct control of protein kinase activity. We now appreciate that Cu directly binds to and influences MEK1/2 and ULK1/2 kinase activity, and show here that reductions in MAPK and autophagic signaling are associated with dampened growth and survival of oncogenic BRAF-driven lung adenocarcinoma cells upon loss of *Ctr1*. Efficient autophagy, clonogenic survival, and tumorigenesis of *BRAF*-mutant cells required ULK1 Cu-binding. Although treatment with canonical MAPK inhibitors resulted in the upregulation of protective autophagy, mechanistically, the Cu chelator tetrathiomolybdate (TTM) was sufficient to target both autophagic and MAPK signaling as a means to blunt BRAF-driven tumorigenic properties. These findings support leveraging Cu chelation with TTM as an alternative therapeutic strategy to impair autophagy and MAPK signaling. As traditional MAPK monotherapies initiate autophagy signaling and promote cancer cell survival.

Implications: We establish that copper chelation therapy inhibits both autophagy and MAPK signaling in $BRAF^{V600E}$-driven lung adenocarcinoma, thus overcoming the upregulation of protective autophagy elicited by canonical MAPK pathway inhibitors.

Introduction

As kinases have the ability to drive oncogenesis, small molecule targeting of kinases has dramatically changed the landscape of cancer-related therapy (1). However, clinical resistance is a major limitation, and thus, identifying new modes of kinase regulation may provide additional targetable vulnerabilities. Although copper (Cu) is traditionally viewed as a static cofactor (2), a newfound role for Cu has emerged within the intracellular signaling circuits necessary for the dynamic temporal and spatial control of cellular processes (3–9). In particular, we have demonstrated that direct Cu binding increases protein kinase activity (4, 6). Moreover, we established that Cu binds directly to MAPK 1/2 (MEK1/2), and that allosteric binding of Cu to MEK1/2 potentiates its phosphorylation of ERK1/2 (3, 4). In turn, depletion of Cu with selective chelating agents, such as tetrathiomolybdate (TTM) used for the treatment of Wilson disease (10), inhibits MEK1/2 kinase activity and slows tumor growth in preclinical models of MAPK-driven cancers (3, 4, 11).

In pursuit of identifying additional Cu-dependent kinases, a sequence homology search of the reported Cu-coordinating residues within MEK1 identified Unc-51–like autophagy-activating kinase 1/2 (ULK1/2) as putative Cu-binding kinases. This finding was supported by the presence of Cu-coordinating amino acids at the same positions within their kinase domains (6). ULK1/2 kinases are involved in the catabolic process of autophagy, and upon metabolic stress, these kinases signal to form double membrane autophagosomes that encapsulate cytoplasmic proteins, lipids, and organelles targeted for degradation in lysosomes (12–15). Interestingly, cellular models and liver tissues from patients with Wilson disease, which demonstrate elevated Cu levels, have more activated autophagy at baseline (16). In line with autophagy activation via enhanced Cu levels, we provided evidence that Cu binding to ULK1 was necessary for ULK1 kinase activity and autophagy signaling to support tumorigenesis in $KRAS^{G12D}$-mutant lung adenocarcinoma (6). Targeting Cu through disruption of the high-affinity Cu transporter 1 (CTR1) or mutagenesis of the ULK1 Cu-binding residues reduced tumor growth kinetics lung tumors driven by $KRAS^{G12D}$. These findings highlighted a novel mode of autophagy regulation and pointed to a potential means of targeting autophagy in cancers that become dependent on this fundamental cellular process for growth and survival.

A number of recent publications emphasize that inhibition of MAPK signaling results in increased autophagic flux and in turn limits the efficacy of MAPK inhibitors and necessities dual targeting of the canonical MAPK pathway and autophagy in tumors (17–19). This finding was confirmed in a number of *KRAS*-mutant and *BRAF*-mutant cancers, including pancreatic, lung, colon, and melanoma (17–19). Given our previous observation that both MAPK pathway activation and autophagy are reduced in oncogenic

[1]Department of Cancer Biology, Perelman School of Medicine, University of Pennsylvania, Philadelphia, Pennsylvania. [2]Abramson Family Cancer Research Institute, Perelman School of Medicine, University of Pennsylvania, Philadelphia, Pennsylvania. [3]Cell and Molecular Biology Graduate Group, Perelman School of Medicine, University of Pennsylvania, Philadelphia, Pennsylvania. [4]Biochemistry and Molecular Biophysics Graduate Group, Perelman School of Medicine, University of Pennsylvania, Philadelphia, Pennsylvania. [5]Pharmacology Graduate Group, Perelman School of Medicine, University of Pennsylvania, Philadelphia, Pennsylvania.

T. Tsang and X. Gu contributed equally as co-authors of this article.

Corresponding Author: Donita C. Brady, Perelman School of Medicine, 421 Curie Boulevard, 612 BRBII/II, Philadelphia, PA 19104. Phone: 215-573-9705; E-mail: bradyd@pennmedicine.upenn.edu

Mol Cancer Res 2022;20:1096–107

doi: 10.1158/1541-7786.MCR-21-0250

KRAS-driven lung tumors in which Cu transport has been ablated, we next turned our attention to cancer driven by its downstream effector murine sarcoma viral oncogene homolog B (BRAF; refs. 6, 20, 21). Notably, lung tumors driven by mutations in *BRAF* have been found to require autophagy for growth (21). Although *BRAF* mutations are rare in lung adenocarcinoma, constituting roughly 3% of all cases, the number of patients diagnosed with BRAF-mutant lung tumors is equivalent to those diagnosed with metastatic melanoma. Moreover, these tumors tend to be more aggressive and resistant to chemotherapy (22). However, favorable responses have been observed in clinical trials with patients harboring $BRAF^{V600E}$-mutant lung tumors treated with kinase inhibitors against BRAF, vemurafenib and dabrafenib, and MEK1/2, trametinib (23, 24). Here, we show that targeting Cu in lung tumors driven by BRAF also suppresses autophagy signaling by mechanistically disrupting Cu-dependent ULK1/2 kinase activity. In contrast with treatment of lung tumor cells driven by oncogenic BRAF with MAPK inhibitors vemurafenib or trametinib in which protective autophagy is upregulated, treatment with the Cu chelator TTM, akin to genetic ablation of the high-affinity Cu transporter *Ctr1*, downregulated autophagy. Because of the increasing dependence on autophagy upon attenuation of MAPK signaling, dual inhibition of both autophagy and MAPK signaling may render a more durable response and thus supporting its potential as a more favorable therapeutic in mutant RAS or RAF-activated cancers (17–19). Given our prior findings that Cu is required in MEK1/2 and ULK1/2 for MAPK activity (3, 4) and autophagic signaling (6), respectively, repurposing Cu chelation to tandemly target these pathways may outline a novel therapeutic avenue for the treatment of $BRAF^{V600E}$-driven lung tumors. Our findings highlight a new approach to autophagy inhibition through depletion of cellular Cu levels or disruption of Cu-kinase interactions to suppress tumorigenesis in BRAF-mutant lung adenocarcinoma.

Materials and Methods

Derivation of cell lines and cell culture

$Braf^{CA/+}$;$Trp53^{flox/flox}$ (BP) $Ctr1^{+/+}$, and $Ctr1^{flox/flox}$ mice have been described previously (4). Tumors were initiated by intranasal infection of mice with adenoviral Cre-recombinase. Cell lines were generated by enzymatic and mechanical dissociation of individual lung tumors arising from either $Ctr1^{+/+}$ or $Ctr1^{flox/flox}$ BP mice harvested at endpoint, either 3 months post intranasal administration of Cre or at moribundity. BP cells were stably infected with retrovirus derived from pBABE or pWZL (see plasmids below) or lentiviruses derived from pLentiCRISPRV2 (*see* plasmids below) using established protocols. A human BRAF-mutant cell line HCC364 was a kind gift from the T.G. Bivona (University of California San Francisco) and did not undergo authentication and NCI-H1666 was purchased from the ATCC. $Ulk1^{-/-}$ immortalized (with SV40) mouse embryonic fibroblasts (MEF) were previously described and provided by S.A. Tooze (Francis Crick Institute; ref. 25). All cell lines were tested for *Mycoplasma* on a monthly basis with the MycoAlert *Mycoplasma* Detection Kit (Lonza). BP cells were authenticated by genotyping PCR and $Ulk1^{-/-}$ MEFs were authenticated by qPCR and Western blot. All cell lines were passaged for no more than 20 times post thaw.

IHC

Sections were deparaffinized, rehydrated, and subjected to epitope retrieval stained with a rabbit anti-LC3B (microtubule-associated protein 1A/11B-light chain 3) antibody (1:1,000; NB100–2220, Novus Biologicals), mouse anti-CCS antibody (1:100; 55561, Santa Cruz Biotechnology), and rabbit anti-p62 antibody (1:1,000; PM04, MBL International) by peroxidase-based detection and counterstaining with hematoxylin using the Leica Bond Rx^m system. Photographs were taken on a Leica DMI6000B inverted light and fluorescent microscope ($\times$20 for quantitation, $\times$5 or $\times$40 for representative images). LC3- and p62-positive staining was assessed in ImageJ. The color deconvolution macro was applied to images whereas tumors were circumscribed with the freehand selection tool on the DAB (3,3′-diaminobenzidine) staining (Color_2) generated window. Using the threshold function, the total area of the tumor in pixels was recorded using the same parameters for each tumor image. Areas staining positive by these parameters were selected and recorded in pixel units. The positive-staining area of the tumor in pixels was divided by the total area of the tumor in pixels to determine the percentage positive-staining area. Statistical analysis of abnormal lung area, the percentage of positive LC3 or positive p62 staining was analyzed using an unpaired, two-tailed Student *t* test in Prism 7 (GraphPad).

Immunoblot analysis

Indicated cell lines were washed with cold PBS and lysed with RIPA buffer containing 1X EDTA-free Halt protease and phosphatase inhibitor cocktail halt protease and phosphatase inhibitors (Thermo Fisher Scientific). The protein concentration was determined by the bicinchoninic acid protein assay (Pierce) using BSA as a standard. Equal amount of lysates were resolved by sodium dodecyl SDS-PAGE using standard techniques, and protein was detected with the following primary antibodies: Rabbit anti-LC3B (1:2,000; NB100–2220, Novus Biologicals), rabbit anti-phospho(S318)-ATG13 (1:1,000; 600–401-C49, Rockland), rabbit anti-ATG13 (1:1,000; 13273, Cell Signaling Technology), rabbit anti-phospho(Ser757)-ULK1 (1:1,000; 6888, Cell Signaling Technology), rabbit anti-ULK1 (1:1,000; 8054, Cell Signaling Technology), rabbit anti-phospho(Thr202/Tyr204)-ERK1/2 (1:1,000; 9101, Cell Signaling Technology), mouse anti-ERK1/2 (1:1,000; 9107, Cell Signaling Technology), mouse anti-CCS (Cu chaperone for superoxide dismutase; 1:1,000; 55561, Santa Cruz Biotechnology), rabbit anti-phospho(S30)-Beclin-1 (1:1,000, 54101, Cell Signaling Technology), rabbit anti-Beclin-1 (1:1,000, 3738, Cell Signaling Technology), mouse anti-HA (1:1,000; 2367, Cell Signaling Technology), and mouse anti–β-actin (1:10,000; 3700, Cell Signaling Technology) followed by detection with one of the horseradish peroxidase–conjugated secondary antibodies: goat anti-rabbit IgG (immunoglobulin G; 1:5,000, 7074, Cell Signaling Technology) or goat anti-mouse IgG (1:5,000, 7076, Cell Signaling Technology), using SignalFire (Cell Signaling Technology) or SignalFire Elite ECL (Cell Signaling Technology) detection reagents. The fold change in the ratio of phosphorylated protein to total protein was measured in Image Studio Lite (LI-CORE Biosciences) software by boxing each band per representative image using the rectangular selection tool and calculating the total area of the band in pixels. The total area of the phosphorylated protein band or modified protein band in pixels was normalized to the total area of the total protein band or β-actin in pixels. The average fold change is shown in figures.

Plasmids

pWZLblasti-$CTR1^{WT}$ (Addgene plasmid #53157; ref. 4), pBABE-puro-mCherry-EGFP-LC3B (Addgene plasmid #22418; ref. 26), pWZLblasti-HA-$ULK1^{WT}$ (6, 13), pWZLblasti-HA-$ULK1^{CBM6}$, pLenti-CRISPRV2puro (Addgene plasmid #52961; ref. 27), and pBABEbleo-FLAG-$BRAF^{V600}$ (Addgene plasmid #53156; ref. 28) were previously described. pLentiCRISPRV2puro-*Atg5*-sgRNA expressing the mouse *Atg5* target sequence 5′-TTCCATGAGTTTCCGATTGA was obtained from GenScript. pLenti-CRISPRV2puro-*Rosa26*-sgRNA

was created to express the mouse *Rosa26* target sequence 5′-CCCGATCCCCTACCTAGCCG. pLentiCRISPRV2puro-*Ctr1*-sgRNA #1 was created to express mouse *Ctr1* target sequence 5′-TTGGTAATCAATACACCTGG. pLentiCRISPRV2puro-*Ctr1*-sgRNA #2 was created to express mouse *Ctr1* target sequence 5′-GGACTCAAGATAGCCCGAGA. pLentiCRISPRV2puro-*Ulk1*-sgRNA was created to express mouse *Ulk1* target sequence 5′-GGCAGTGTACGGTTCCGAGG. pLentiCRISPRV2puro-*CTR1*-sgRNA #1 was created to express human *CTR1* target sequence 5′-TTGGTGATCAATACAGCTGG. pLentiCRISPRV2puro-*CTR1*-sgRNA #2 was created to express human *CTR1* target sequence 5′-GTGATGGTGAGAAGGTTGCA. pBABE-puro-HA-RAB33B$^{Q92\ L}$ was created by PCR subcloning RAB33B$^{Q92\ L}$ from pcDNA3.23-RAB33B^{Q92L}-BirA*-HA-MAO (Addgene plasmid #128920; ref. 29) with primers designed to include an N-terminal HA-tag.

Reverse transcriptase-PCR and Reverse transcriptase-quantitative PCR

For RT-qPCR, RNA was purified from tumor cell lines and reverse transcribed to cDNA as previously described and then quantified using a TaqMan probe Mm00558247_m1 to detect mouse *Ctr1*, Hs00977266_g1 to detect human *CTR1*, Mm00437238_m1 to detect mouse *Ulk1*, Mm01277042_m1 to detect mouse TATA-binding protein (*Tbp*), or Hs00427620_m1 to detect human *TBP* using the ViiA 7 Real-Time PCR System. Relative mRNA expression levels were normalized to either mouse *Tbp* or human *TBP* and analyzed using comparative delta-delta cycle threshold (C_t) method.

Clonogenic survival assays

Cells were seeded at 80,000 cells/well in 12-well plates and 24 hours later washed with PBS and media were changed to Earle's Balanced Salt Solution (EBSS, E2888, Sigma-Aldrich). After 24, 48, or 72 hours, EBSS was removed and replaced with DMEM (11965118, Gibco) supplemented with 1% penicillin–streptomycin (5,000 U/mL, 15070063, Gibco) and 10% Hyclone Cosmic Calf Serum (SH3008703, Cytiva). For experiments involving drug treatments, drugs were added at the indicated dose(s) and maintained in the culture medium throughout the experiment 24 hours after seeding. Cells were fixed and stained with 500 μL crystal violet solution (0.5%) for 15 minutes after recovery in replenished medium for 72 hours. Cells were washed with deionized water and plates allowed to dry before images were taken with the Bio-Rad Chemidoc Imaging System. Stain was removed from cells by adding 1 mL of 10% acetic acid/well and plates were rocked for 20 minutes at room temperature. Samples from each well were transferred to a 96-well plate, and 590 nmol/L absorbance was read on a Synergy HT plate reader (BioTek Instruments). Statistical analysis of 590 nmol/L absorbance was performed using a two-way ANOVA followed by Tukey's multi-comparison test in Prism 7 (GraphPad).

Drugs

Bafilomycin A1 (BAF, Cayman Chemical), Vemurafenib (ChemieTek), trametinib (Selleck Chemicals), and ammonium TTM, abbreviated as TTM (Sigma-Aldrich), were dissolved in dimethyl sulfoxide.

Mouse xenografts

Immortalized, transformed MEFs, seeded at a density 10^7 cells, resuspended in PBS were injected subcutaneously into flanks of SCID/beige mice (Strain 250, Charles River Laboratory) as previously described (30). All studies were approved by the University of Pennsylvania Institutional Animal Care and Use Committee. Statistical analysis of tumor volumes and tumor weights at end point was performed using an unpaired, one-tailed Student *t* test in Prism 7 (GraphPad).

Electron Microscopy

Tumor tissue was processed and prepared for ultrastructure analysis by the Electron Microscopy Resource Laboratory (EMRL) at the University of Pennsylvania. Specimens were imaged on a JEOL JEM 1010 transmission electron microscope equipped with a 2k × 2k advanced microscopy technique chare-coupled device camera that uses a tungsten filament as its electron source. Autophagosome numbers per cell were manually counted by a researcher blinded to the treatment group. Statistical analysis of autophagosome number was analyzed using an unpaired, two-tailed Student *t* test in Prism 7 (GraphPad).

Statistical analysis and reproducibility

Data are represented as the mean ± s.e.m. The sample size (*n*) indicates biologically independent experiments, biologically independent samples, biologically independent animals, individual cells, or fields of view. To ensure reproducibility, data were derived from the following: for biologically independent experiments, at least three independent experiments; for biologically independent samples, at least nine independent samples from at least three independent experiments; for biologically independent animals, at least four independent animals; for fields of view, at least 18 fields of view from two biologically independent experiments. Statistical significance was typically determined using an unpaired, one-tailed Student *t* test, an unpaired, two-tailed Student *t* test, paired, two-tailed Student *t* test, a one-way ANOVA followed by a Tukey's multi-comparisons test, a two-way ANOVA followed by a Sidak's multi-comparisons test, or a two-way ANOVA followed by Tukey's multi-comparisons test to determine significant in Prism 7 (GraphPad).

Data availability

The data generated in this study are available upon request from the corresponding author.

Results

Ablation of *Ctr1* impairs autophagic flux and signaling in *BRAF* mutation-positive lung adenocarcinoma

Previous work demonstrated that genetic ablation of the Cu transporter *Ctr1* reduces the development of BRAF^{V600E}-driven lung tumors, resulting in a survival advantage (4). Importantly, oncogenic BRAF^{V600E}-driven lung adenocarcinomas depend on autophagy for tumor maintenance (21). To examine whether autophagy was impaired in Cu-deficient BRAF^{V600E}-driven lung adenocarcinoma, we used tumors from mice harboring floxed conditional null or wild-type *Ctr1* alleles (31) crossed into a *Braf*$^{CA/+}$;*Trp53*$^{flox/flox}$ (BP) background (refs. 4, 32; Supplementary Fig. S1A). The established *Ctr1*$^{flox/flox}$ BP mice tumors had decreased LC3-positiive staining and increased p62-positive staining, suggesting suppressed autophagy (**Fig. 1A–D**). Cu levels correlate with CCS stability, with increased CCS stability correlating to lower Cu availability and vice versa (33). The *Ctr1*$^{flox/flox}$ BP mice tumors exhibited increased CCS staining indicative of decreased tumor Cu levels (**Fig. 1E** and **F**). To interrogate whether the requirement for Cu to induce autophagy in the BRAF^{V600E} lung tumors was associated with altered ULK1/2 signaling, we established lung adenocarcinoma cell lines from *Ctr1*$^{+/+}$ and *Ctr1*$^{flox/flox}$ BP mice (Supplementary Fig. S1A). First, autophagic flux was measured by Western blot analysis of LC3 processing from cleaved

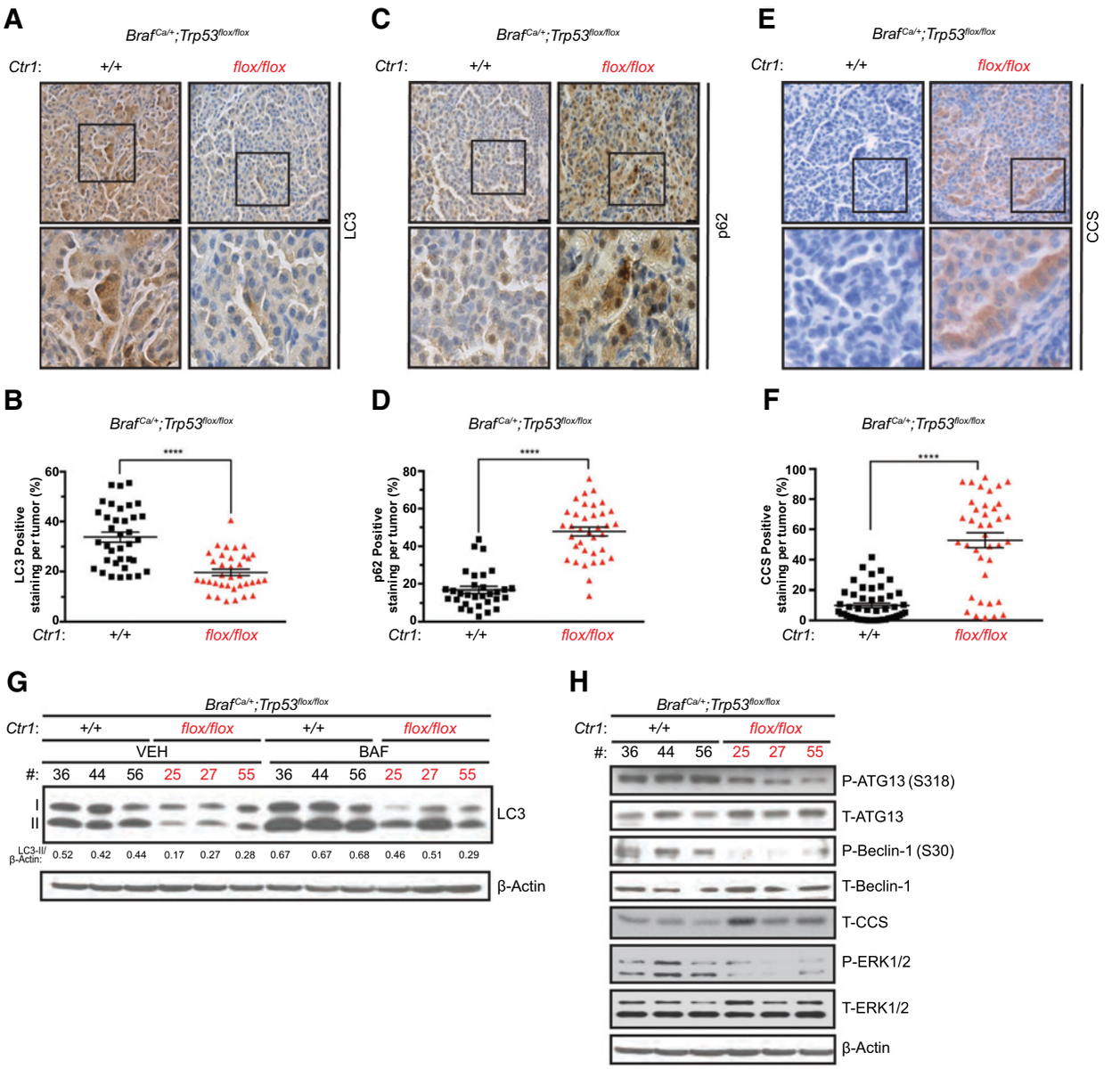

Figure 1.

Ablation of *Ctr1* impairs autophagic flux and signaling in *BRAF* mutation-positive lung adenocarcinoma. **A, C,** and **E,** Representative images of immunohistochemical detection of LC3 (**A**), p62 (**C**) or CCS (**E**) of lung tumors from $Ctr1^{+/+}$ or $Ctr1^{flox/flox}$ $Braf^{CA/+};Trp53^{flox/flox}$ (BP) mice; scale bar, 50 μm. **B, D,** and **F,** Scatter dot at mean ± s.e.m. percentage of (%) LC3-positive staining ($n = 36$; **B**), percentage of p62-positive staining ($Ctr1^{+/+}$, $n = 31$ and $Ctr1^{flox/flox}$, $n = 36$; **D**), or percentage of CCS-positive staining ($Ctr1^{+/+}$, $n = 31$ and $Ctr1^{flox/flox}$, $n = 36$; **F**) per lung tumor from $Ctr1^{+/+}$ (black squares) versus $Ctr1^{flox/flox}$ (red triangles) BP mice. Results were compared using an unpaired, one-tailed Student *t* test; ****, $P < 0.0001$. $n \geq 31$. **G** and **H,** Immunoblot detection of LC3-I, LC3-II, phosphorylated (P) ATG13, total (T) ATG13, P-Beclin-1, T-Beclin-1, T-CCS, P-ERK1/2, T-ERK1/2, or β-actin in either $Ctr1^{+/+}$ (#36, #44, #56) or $Ctr1^{flox/flox}$ (#25, #27, #55) BP lung adenocarcinoma cell lines treated with vehicle (VEH) or bafilomycin (BAF) for 1 hour. Quantification: ΔLC3-II/β-actin.

LC3 (LC3-I) to phosphatidylethanolamine-conjugated LC3 (LC3-II) upon disruption of autophagic flux using the lysosomal v-ATPase inhibitor bafilomycin. The genetic ablation of *Ctr1* reduced LC3-I processing, suggesting decreased autophagic flux (**Fig. 1G**). Mechanistically, our prior findings demonstrated that Cu binds to and directly modulates the kinase activity of both MEK1/2 and ULK1/2 (3, 4, 6). In agreement, loss of *Ctr1* reduced ULK1/2-mediated phosphorylation of ATG13^{S318} and Beclin-1^{S30} and MEK1/2-mediated phosphorylation of ERK1/2 when compared with Cu-replete $Ctr1^{+/+}$ cells (**Fig. 1H**; refs. 12, 13, 34, 35). To investigate the relationship between Cu and autophagy in the context of endogenous oncogenic *BRAF* mutations, *CTR1* knockout human *BRAF* mutation-positive lung adenocarcinoma cell lines were generated via CRISPR/Cas9 (Supplementary Fig. S1B) and found to have reduced autophagic flux

and dampened MAPK pathway activation (Supplementary Fig. S1C and S1D). Together, our findings indicate that a reduction in Cu levels through *Ctr1* loss suppresses autophagic flux and signaling, suggesting that Cu depletion dampens oncogenic BRAF-mediated autophagy that is necessary for tumor growth.

Reduced Cu influx impairs survival after starvation of *BRAF*-mutant lung tumor cells

Deficiencies in autophagy impair the survival of BRAF-driven lung tumor cells in starvation conditions where amino acids have been depleted (21). To test whether altering Cu availability affects

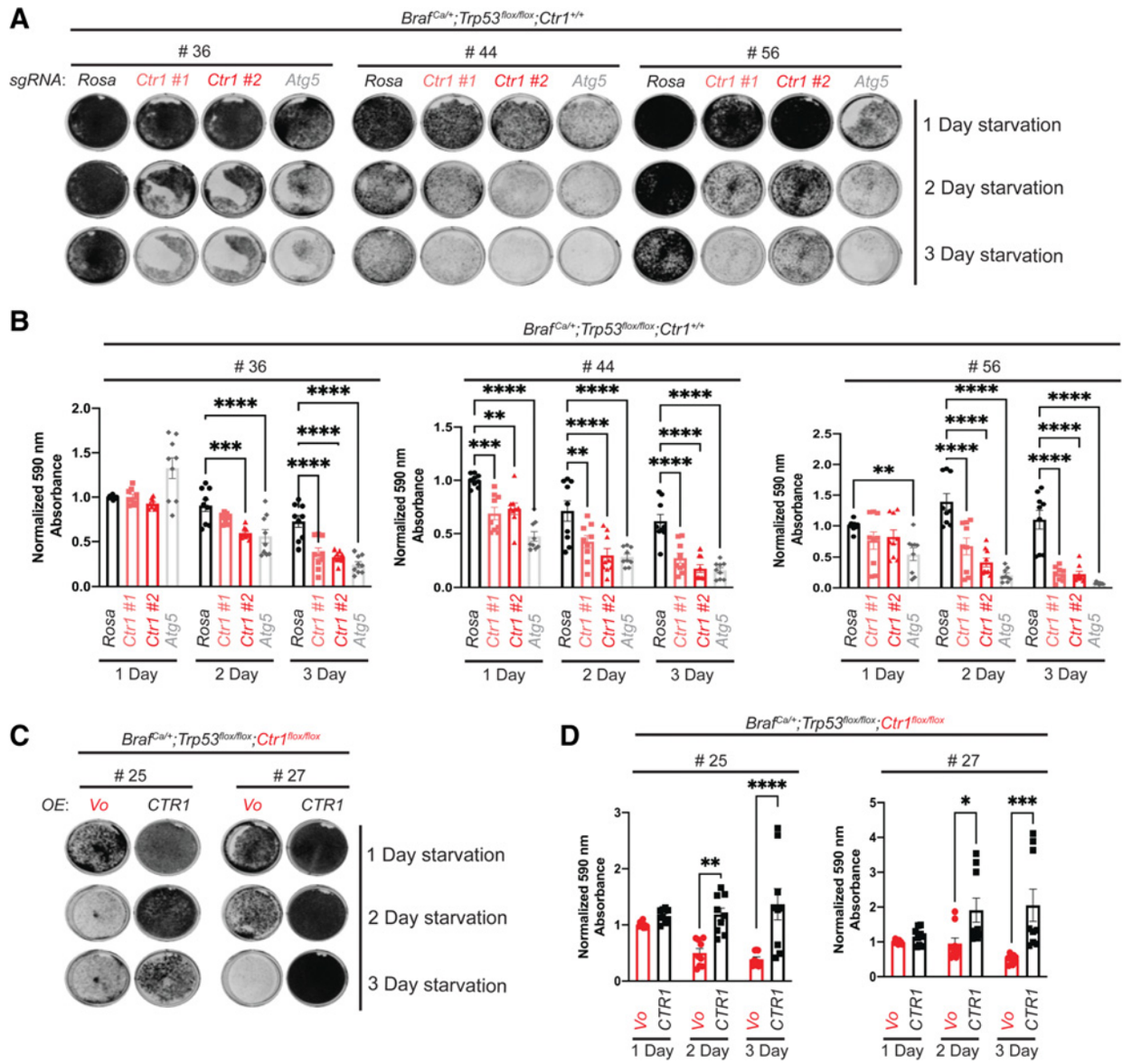

Figure 2.

Reduced Cu influx impairs survival after starvation of *BRAF*-mutant lung tumor cells. **A,** Representative crystal violet images of *Braf*$^{CA/+}$;*Trp53*$^{flox/flox}$ (BP) #36, BP #44, and BP #56 cells stably expressing *sgRNA* against *Rosa*, *Ctr1* (*#1* or *#2*), or *Atg5* after 1, 2, or 3 days of starvation followed by recovery in nutrient-replete media. **B,** Scatter dot plot with bar at mean absorbance of extracted crystal violet at 590 nmol/L ± s.e.m. of BP #36, BP #44, and BP #56 cells stably expressing *sgRNA* against *Rosa*, *Ctr1* (*#1* or *#2*), or *Atg5* after 1, 2, or 3 days of starvation followed by recovery in nutrient-replete media normalized to *Rosa*, 1 day control. Results were compared using a two-way ANOVA followed by Tukey's multi-comparisons test. BP #36, *n* represents number of biologically independent samples; *Rosa* $n = 9$, *#1* $n = 9$, *#2* $n = 9$; ***, $P \leq 0.0006$; and ****, $P < 0.0001$. BP #44, *n* represents number of biologically independent samples; *Rosa* $n = 9$, *#1* $n = 9$, *#2* $n = 9$; **, $P \leq 0.0013$; ***, $P = 0.0004$; and ****, $P < 0.0001$. BP #56, *n* represents number of biologically independent samples; *Rosa* $n = 9$, *#1* $n = 9$, *#2* $n = 9$; **, $P = 0.0064$; and ****, $P < 0.0001$. **C,** Representative crystal violet images of BP #25 and BP #27 cells stably expressing an empty vector (Vo) or CTR1 after 1, 2, or 3 days of starvation followed by recovery in nutrient-replete media. **D,** Scatter dot plot with bar at mean absorbance of extracted crystal violet at 590 nmol/L ± s.e.m. of BP #25 and BP #27 cells stably expressing an empty vector (Vo) or CTR1 after 1, 2, or 3 days of starvation followed by recovery in nutrient-replete media normalized to Vo, 1 day control. Results were compared using a two-way ANOVA followed by Tukey's multi-comparisons test. BP #25, *n* represents number of biologically independent samples; Vo $n = 9$, CTR1 $n = 9$; **, $P = 0.0015$; and ****, $P < 0.0001$. BP #27, *n* represents number of biologically independent samples; Vo $n = 9$, CTR1 $n = 9$; *, $P = 0.0424$; and ****, $P < 0.0001$.

autophagy machinery and, in turn, survival in starvation conditions, BP cells were starved for either 1, 2, or 3 days and then allowed to recover in nutrient-replete media for 3 days before assessing clonogenic survival (Supplementary Fig. S2A). To investigate the contribution of Cu on clonogenic survival, the Cu transporter *Ctr1* was knocked out by CRISPR/Cas9 in mouse $Ctr1^{+/+}$ BP lung tumor cells (Supplementary Fig. S2B). The clonogenic survival of *Ctr1*-deficient BP cells was significantly decreased to an extent similar to that of the CRISPR/Cas9 knockout of the essential autophagy gene *Atg5* (**Fig. 2A** and **B**; Supplementary Fig. S2B and S2C), which is required for the ubiquitin-like conjugation system that lipidates LC3 (36). Parallel results were observed in both Cu-replete conditions in which Cu-deficient BP cells were transduced to stably express the high affinity Cu transporter CTR1 in $Ctr1^{flox/flox}$ BP lung tumor cells (**Fig. 2C** and **D**; Supplementary Fig. S2D). In agreement with BP lung tumor cell lines isolated from genetically engineered mouse model, *CTR1* knockout human *BRAF* mutation-positive lung adenocarcinoma cell lines exhibited reduced clonogenic survival post-starvation when compared with control cells (Supplementary Fig. S2E–S2H). This observation suggests that Cu is required for proper function of autophagy machinery, which is necessary for survival post-starvation.

Restoration of autophagic flux downstream of ULK1/2 partially rescues survival after starvation of Cu-deficient *BRAF*-mutant lung cancer cells

To ascertain the extent to which Cu binding to the MAPK kinases MEK1/2 contributes to the inability of Cu-deficient *BRAF*-mutant lung cancer cells to survive starvation, we first expressed a gain-of-function (GOF) ERK2 mutant, which bypasses the ability of Cu to influence MEK1/2 activity in $Ctr1^{flox/flox}$ BP cells (Supplementary Fig. S3A and S3B; ref. 4), and as a result increased phosphorylated of ERK1/2 but failed to elevate LC3-II levels in cells devoid of significant Cu transport (Supplementary Fig. S3A and S3B). Importantly, expression of $ERK2^{GOF}$ was not sufficient to rescue the decreased clonogenic survival of the Cu transporter defective $Ctr1^{flox/flox}$ *BRAF*-mutant lung cancer cells (**Fig. 3A** and **B**), which suggests that the survival of these lung cancer cells depends on autophagy in an MAPK-independent fashion. In agreement with impaired autophagy in the Cu-deficient BP lung cancer cells influencing clonogenic survival, expression of a constitutively active mutant of RAB33B, which recruits the ATG16L1 complex to the growing phagophore downstream of ULK1/2 to induce LC3 lipidation (37), was sufficient to reestablish autophagic flux and restore survival after starvation to a similar degree as reexpression of CTR1 in $Ctr1^{flox/flox}$ BP lung cancer cells (**Fig. 3C** and **D**; Supplementary Fig. S3C and S3D). Our collective results demonstrate that the dependence of BRAF-driven tumors on Cu transport is in part due to insufficient autophagy necessary for tumor cell survival in the absence of nutrients.

A Cu-ULK1 interaction is required for the induction of autophagic signaling

To mechanistically interrogate the contribution of Cu-binding to ULK1 signal transduction and initiation of autophagy in $BRAF^{V600E}$ lung tumors, we mutated the conserved primary sequence of ULK1 to mimic that the ***C***u-binding mutant (CBM) of MEK1 (4), consisting of H136, M188, and H197 to alanine mutations. Generation of the $ULK1^{CBM}$ resulted in reduced *in vitro* capacity to bind to a Cu-charged resin and phosphorylate ATG13 (6). To investigate the impact of the loss of ULK1 Cu-binding on autophagic flux and signaling in $BRAF^{V600E}$ tumorigenesis, *Ulk1* was knocked out by CRISPR/Cas9 in a $Ctr1^{+/+}$ BP mutant lung adenocarcinoma cell line (Supplementary Fig. S4A). In agreement with Cu-dependent ULK1 kinase activity, only the expression of $ULK1^{WT}$, but not $ULK1^{CBM}$, in *Ulk1*-deficient BP cells could increase processing of LC3-I to LC3-II and $ATG13^{S318}$ phosphorylation (**Fig. 4A** and **B**). Directly upstream of ULK1 is the major nutrient sensing complex mTORC1 that regulates ULK1 via phosphorylation at $ULK1^{S757}$, resulting in ULK1 kinase inhibition when cellular energetics are favorable under conditions such as amino acid and growth factor repletion (12–14, 34, 38). In contrast with a decrease in $ATG13^{S318}$ phosphorylation in $ULK1^{CBM}$ versus $ULK1^{WT}$ reconstituted *Ulk1*-deficient BP cells, $ULK1^{S757}$ phosphorylation remains unchanged, suggesting that Cu binding is required for ULK1 activity but not upstream ULK1 regulation by mTORC1 itself (**Fig. 4B**). To investigate the contribution of ULK1 Cu-binding on survival after starvation, clonogenic survival was assessed in CRISPR/Cas9 *Ulk1* knockout $Ctr1^{+/+}$ BP cells reconstituted with empty vector (Vo), $ULK1^{WT}$, or $ULK1^{CBM}$ (**Fig. 4C** and **D**). As expected, loss of *Ulk1* reduced survival after starvation; however, survival was enhanced upon re-expression of $ULK1^{WT}$ and not $ULK1^{CBM}$. Thus, our results highlight the necessity of Cu in the survival of BRAF-mutant lung tumor cells through ULK1 regulation of autophagy. Together, these findings indicate that Cu binding is required to restore autophagy downstream of ULK1 in $BRAF^{V600E}$-driven lung tumors.

Disruption of the Cu–ULK1 interaction alters $BRAF^{V600E}$ tumorigenesis

To translate our findings that Cu binding to ULK1 is required for autophagy in BRAF-driven tumorigenesis, we tested and found that disrupting ULK1 Cu binding was associated with reduced tumor growth kinetics and endpoint tumor weight of $BRAF^{V600E}$-transformed, CRISPR/Cas9 knocked out of *Ulk1* immortalized MEFs stably expressing ULK^{CBM} compared with $ULK1^{WT}$ (**Fig. 5A**–**C**). To then investigate whether these findings could be extended to endogenous oncogenic BRAF tumorigenesis, *Ulk1* was knocked out by CRISPR/Cas9 in mouse BP lung adenocarcinoma cell lines that were rescued by the stable re-expression of either $ULK1^{WT}$ or $ULK1^{CBM}$. $ULK1^{CBM}$ exhibited decreased tumor kinetics and endpoint tumor weight relative to $ULK1^{WT}$ *Ulk1*-deficient BP subcutaneous tumor growth (**Fig. 5D** and **E**). Molecularly, the $ULK1^{CBM}$-expressing *Ulk1*-deficient BP tumors had reduced autophagosome number, indicative of dampened autophagy (**Fig. 5G** and **H**). Together, these findings support a mechanism to regulate ULK1 activity through Cu binding to promote oncogene-driven autophagy necessary for tumorigenesis.

Cu chelation alters the protective autophagy resulting from MAPK pathway inhibition

Several studies recently reported that MAPK pathway inhibition in KRAS- or BRAF-mutant cancers results in the upregulation of protective autophagy through an ULK1-dependent signaling cascade, augmenting the survival of cancer cells (17–19). These studies indicate that dual targeting of the canonical MAPK pathway and autophagy may be required for anti-tumorigenic activity in targeting MAPK-dependent tumors harboring KRAS or BRAF mutations. Given that targeting Cu has been shown to inhibit MAPK activity through MEK1/2 (3, 4) and autophagy signaling through ULK1/2 (6), the efficacy of repurposing a Cu chelator TTM used for the treatment of Cu overload in Wilson disease (10) in dually suppressing MAPK and autophagy signaling was evaluated. In parallel, singular suppression of MAPK signaling was assessed via the canonical small molecule BRAF and MEK1/2 inhibitors—vemurafenib and trametinib, respectively—in

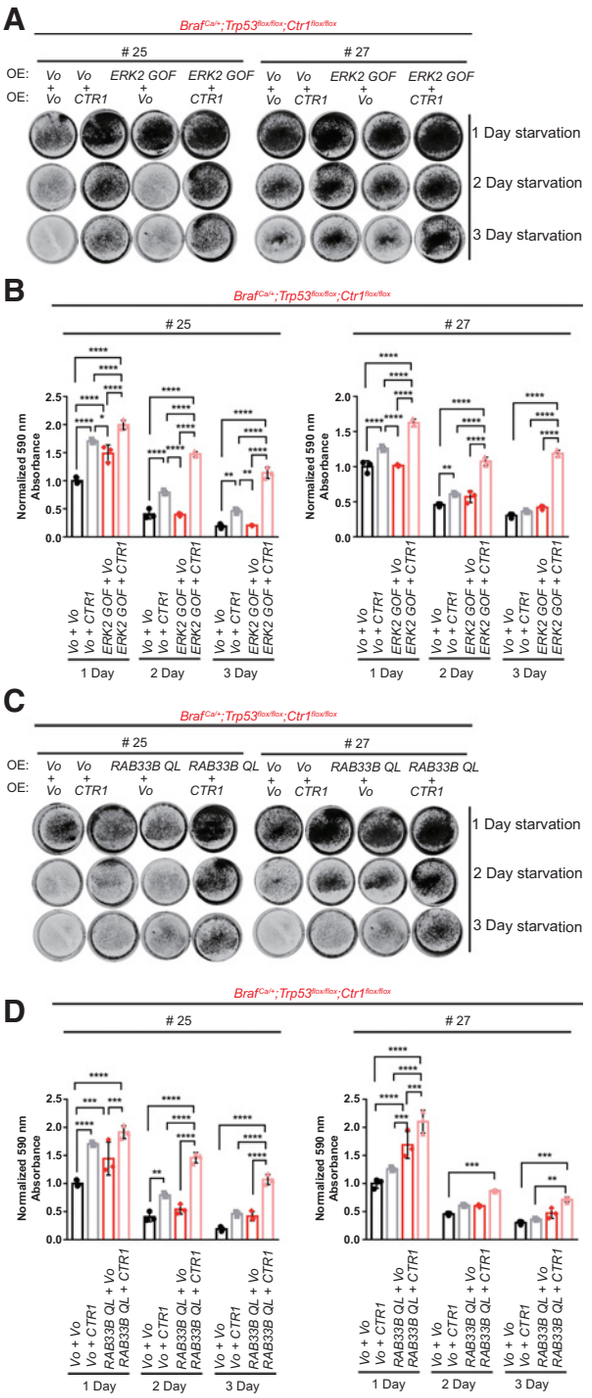

Figure 3.

Restoration of autophagic flux downstream of ULK1/2 partially rescues clonogenic survival after starvation of Cu-deficient *BRAF*-mutant lung cancer cells. **A,** Representative crystal violet images of $Ctr1^{flox/flox}$ (#25, #27) $Braf^{CA/+};Trp53^{flox/flox}$ (BP) lung adenocarcinoma cell lines stably expressing empty vector (Vo) or $CTR1^{WT}$ and empty vector (Vo) or $ERK2^{GOF}$ after 1, 2, or 3 days of starvation followed by recovery in nutrient-replete media. **B,** Scatter dot plot with bar at mean absorbance of extracted crystal violet at 590 nmol/L ± s.e.m. of $Ctr1^{flox/flox}$ (#25, #27) BP lung adenocarcinoma cell lines cells stably expressing empty vector (Vo) or $CTR1^{WT}$ and empty vector (Vo) or $ERK2^{GOF}$ after 1, 2, or 3 days of starvation followed by recovery in nutrient-replete media normalized to $Ctr1^{flox/flox}$, 1 day control. Results were compared using a two-way ANOVA followed by Tukey's multi-comparisons test. BP #25, *n* represents number of biologically independent samples; $Vo + Vo$ $n = 3$, $Vo + CTR1$ $n = 3$, $ERK2^{GOF} + Vo$ $n = 3$, $ERK2^{GOF} + CTR1$ $n = 3$; *, $P = 0.0163$; ***, $P < 0.0006$; and ****, $P < 0.0001$. BP #27, *n* represents number of biologically independent samples; $Vo + Vo$ $n = 3$, $Vo + CTR1$ $n = 3$, $ERK2^{GOF} + Vo$ $n = 3$, $ERK2^{GOF} + CTR1$ $n = 3$; **, $P = 0.0095$; and ****, $P < 0.0001$. **C,** Representative crystal violet images of $Ctr1^{flox/flox}$ (#25, #27) $Braf^{CA/+};Trp53^{flox/flox}$ (BP) lung adenocarcinoma cell lines stably expressing empty vector (Vo) or $CTR1^{WT}$ and empty vector (Vo) or $RAB33B^{QL}$ after 1, 2, or 3 days of starvation followed by recovery in nutrient-replete media. **D,** Scatter dot plot with bar at mean absorbance of extracted crystal violet at 590 nmol/L ± s.e.m. of BP #25 and BP #27 cells stably expressing empty vector (Vo) or $CTR1^{WT}$ and empty vector (Vo) or $RAB33B^{QL}$ after 1, 2, or 3 days of starvation followed by recovery in nutrient-replete media normalized to $Ctr1^{flox/flox}$, 1 day control. Results were compared using a two-way ANOVA followed by Tukey's multi-comparisons test. BP #25, *n* represents number of biologically independent samples; $Vo + Vo$ $n = 3$, $Vo + CTR1$ $n = 3$, $RAB33B^{QL} + Vo$ $n = 3$, $RAB33B^{QL} + CTR1$ $n = 3$; **, $P = 0.0050$; and ***, $P = 0.0010$; and ****, $P < 0.0001$. BP #27, *n* represents number of biologically independent samples; $Vo + Vo$ $n = 3$, $Vo + CTR1$ $n = 3$, $RAB33B^{QL} + Vo$ $n = 3$, $RAB33B^{QL} + CTR1$ $n = 3$; ***, $P = 0.0004$; and ****, $P < 0.0001$.

BRAF lung cancer cells (**Fig. 6A**; Supplementary Fig. S5A–S5D). Phosphorylation of $ERK1/2^{T202/Y204}$ was used as a readout for MAPK activity and CCS protein stability was used to monitor Cu levels (33) upon treatment of $BRAF^{V600E}$-mutant lung cancer cells with trametinib, vemurafenib, or TTM. In alignment with previous publications (17–19), MAPK pathway inhibition with the canonical MAPK inhibitors vemurafenib or trametinib resulted in autophagy upregulation as evidence by increased processing of LC3-I to LC3-II, whereas treatment with the Cu chelator TTM decreased LC3-II accumulation in $Ctr1^{+/+}$ BP lung tumor cells (**Fig. 6B**). ULK1 phosphorylation of substrates ATG13 and Beclin-1 were reduced in TTM treated but not trametinib or vemurafenib-treated BP cells, indicating that reduced Cu levels dampen ULK1 kinase activity and in turn, autophagy signaling (**Fig. 6C**). These findings suggest that Cu chelation may circumvent the onset of protective autophagy through dual inhibition of both MAPK and autophagic signaling axes. Importantly, survival after starvation was also diminished in TTM-treated relative to trametinib- or vemurafenib-treated $Ctr1^{+/+}$ BP cells (**Fig. 6D** and **E**). Collectively, these data suggest that Cu chelation treatment can overcome the onset of protective autophagy, through inhibition of ULK1 kinase activity, which may be limiting the efficacy of canonical MAPK inhibitors in treating $BRAF^{V600E}$-driven lung cancer.

Discussion

Here, we identified that the essential micronutrient Cu directly modulates the activities of the autophagic kinases ULK1/2 in driving autophagy in $BRAF^{V600E}$-driven lung adenocarcinoma. The catabolic process of autophagy is complex and how it is hijacked by cancers is context dependent. In lung tumors driven by $BRAF^{V600E}$, autophagy has been shown to support tumorigenesis through preserving mitochondrial metabolism as loss of the essential autophagy gene *Atg7* converts adenomas and adenocarcinomas to benign oncocytomas with defective mitochondria (21). Currently, chloroquine (CQ) and its analog hydroxychloroquine (HCQ) are the only clinically approved autophagy inhibitors (39). These antimalarial agents were identified

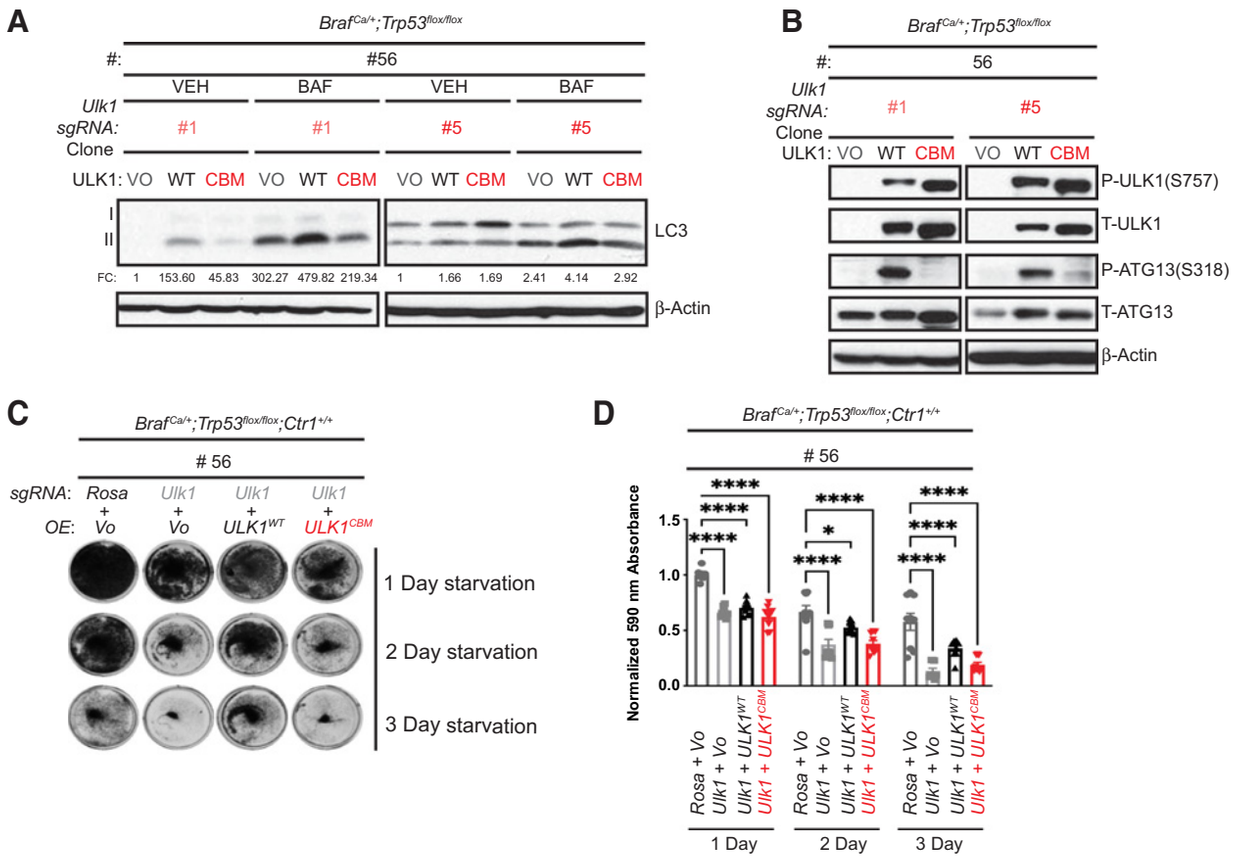

Figure 4.

A Cu–ULK1 interaction is required for autophagic signal induction. **A,** Immunoblot detection of LC3-I, LC3-II, or β-actin from BP #56 sgRNA clones against *Ulk1* (#1 or #5) with empty vector (Vo), ULK1^{WT}, or ULK1^{CBM} treated with vehicle (VEH) or bafilomycin (BAF). Quantification: ΔLC3-II/ β-actin normalized to Vo VEH control. **B,** Immunoblot detection of phosphorylated (P) ULK1, total (T) ULK1, P-ATG13, T-ATG13, or β-actin from BP #56 sgRNA clones against *Ulk1* (#1 or #5) with Vo, ULK1^{WT} or ULK1^{CBM}. **C,** Representative crystal violet images of BP #56 cells stably expressing *sgRNA* against *Rosa* or *Ulk1* reconstituted with Vo, ULK1^{WT}, or ULK1^{CBM} after 1, 2, or 3 days of starvation followed by recovery in nutrient-replete media. **D,** Scatter dot plot with bar at mean absorbance of extracted crystal violet at 590 nmol/L ± s.e.m. of BP #56 cells stably expressing *sgRNA* against *Rosa* or *Ulk1* reconstituted with Vo, ULK1^{WT}, or ULK1^{CBM} after 1, 2, or 3 days of starvation followed by recovery in nutrient-replete media normalized to *Rosa* + *Vo*, 1 day control. Results were compared using a two-way ANOVA followed by Sidak's multi-comparisons test. BP #56, *n* represents number of biologically independent samples; *Rosa* + *Vo* $n = 9$, *Ulk1* + *Vo* $n = 9$, *Ulk1* + *ULK1^{WT}* $n = 9$, *Ulk1* + *ULK1^{CBM}* $n = 9$; *, $P < 0.04$; and ****, $P < 0.001$.

to increase lysosomal pH but have many limitations, including some long-term toxicities (40, 41) and inconsistencies in autophagy inhibition (42). Thus, more selective and potent inhibitors have been developed and are undergoing clinical investigation, including another derivative of CQ, Lys05, and more selective inhibitors targeting specific autophagy machinery, including ULK, pan PI3K, VPS34, and ATG (39).

We have now identified that integral protein kinases MEK1/2 (3, 4) and ULK1/2 (6), within the MAPK and autophagy signaling cascades, respectively, are targets of Cu. Interestingly, the inhibition of the MAPK pathway results in the upregulation of protective autophagy and recently dual inhibition of both pathways has been shown to have a more durable therapeutic response in RAS-driven cancers (17–19). Given the necessity of Cu for ULK1/2 activity (6), the chelation of Cu has the unique capacity to stave the onset of protective autophagy manifested from MAPK inhibition alone that promotes the survival of RAS-driven cancers. In KRAS^{G12D} (6) and now BRAF^{V600E}-driven lung adenocarcinoma, we demonstrate that autophagy can be blunted through depleting cellular Cu levels through either targeting the high affinity Cu transporter, CTR1, or systemic chelation using the Cu specific chelator TTM (**Figs. 1** and **6**). Mechanistically, Cu depletion dampens MEK1/2 activity as readout by ERK1/2 phosphorylation and ULK1/2 activity as read out by ATG13 and Beclin-1 phosphorylation (**Figs. 1** and **6**). Although autophagic flux was enhanced upon treatment of BRAF^{V600E} mutant lung adenocarcinoma cells with MAPK inhibitors, including trametinib and vemurafenib, treatment with TTM reduced autophagy flux and, in turn, limited the clonogenic survival of cells after starvation (**Fig. 6**). Specifically, targeting the Cu binding of ULK1/2 reduced autophagy signaling and growth of lung tumors driven by BRAF^{V600E} (**Figs. 4** and **5**).

Our findings that genetically reducing Cu influx inhibits ULK1/2 signaling, autophagy, and tumor growth driven by oncogenic BRAF, suggests that Cu-chelation therapy, which is generally safe, economically favorable, and given daily to patients with Wilson disease to manage Cu levels (43), could be repurposed as an inhibitor for ULK1/2 to block autophagy in cancer. Admittedly, in order for

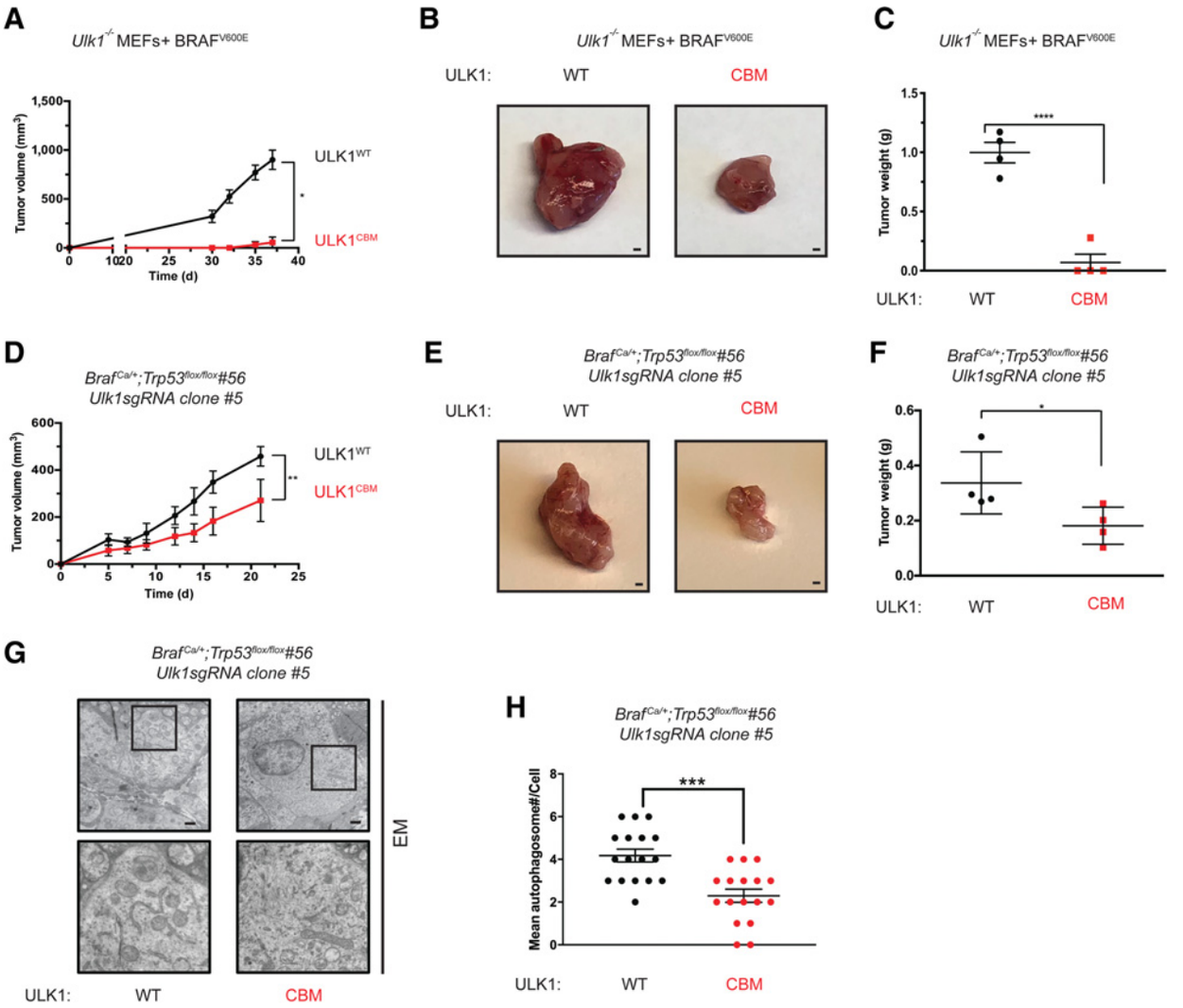

Figure 5.

Disruption of the Cu–ULK1 interaction alters BRAF^{V600E} tumorigenesis. **A,** Mean tumor volume (mm^3) ± s.e.m. versus times (days) in mice injected with immortalized transformed BRAF^{V600E} ULK1$^{-/-}$ MEFs. $n = 4$ biologically independent animals. Results were compared using a paired, one-tailed Student *t* test. ULK1^{WT} versus ULK1^{CBM}; **, $P = 0.0381$. **B,** Representative dissected tumors from mice injected with immortalized transformed BRAF^{V600E} ULK1$^{-/-}$ MEFs; scale bar, 100 μm. **C,** Scatter dot plot at mean tumor weight (g) ± s.e.m. of immortalized transformed BRAF^{V600E} ULK1$^{-/-}$ MEF tumors at endpoint. $n = 4$ biologically independent animals. Results were compared using an unpaired, one-tailed Student *t* test; ****, $P < 0.0001$. **D,** Mean tumor volume (mm^3) ± s.e.m. versus times (days) in mice injected with *Braf$^{CA/+}$;Trp53$^{flox/flox}$* (BP) cells. $n = 4$ biologically independent animals. Results were compared using an unpaired, one-tailed Student *t* test. ULK1^{WT} versus ULK1^{CBM}; **, $P = 0.044$. **E,** Representative dissected tumors from mice injected with BP cells; scale bar, 100 μm. **F,** Scatter dot plot at mean tumor weight (g) ± s.e.m. of BP tumors at endpoint. $n = 4$ biologically independent animals. Results were compared using a paired, one-tailed Student *t* test; *, $P = 0.0277$. **G,** Representative images of electron microscopy (EM) of tumors from mice injected with BP cells expressing *sgRNA* against *Ulk1* reconstituted with *HA-ULK1^{WT}* or *HA-ULK1^{CBM}* (scale bar, 1 μm). **H,** Scatter dot at mean ± s.e.m. of autophagosome number per tumor cell (*HA-ULK1^{WT}*, $n = 25$ images; *HA-ULK1^{CBM}*, $n = 21$ images. Results were compared using an unpaired, two-tailed Student *t* test; ***, $P < 0.0001$. Results were compared using a two-way ANOVA followed by Tukey's multi-comparisons test. BP #25, *n* represents number of biologically independent samples; Vo $n = 9$, CTR1 $n = 9$; **, $P = 0.0015$; and ****, $P < 0.0001$. BP #27, *n* represents number of biologically independent samples.

treatment with the Cu chelator TTM to be well tolerated in clinical trials of patients with breast cancer (44), TTM dosing was benchmarked to serum ceruloplasmin activity to avoid excessively low Cu levels and associated dose-limiting side effects like anemia and neutropenia. Thus, the clinical efficacy of repurposing Cu chelators to target autophagy in cancers remains to be determined. More broadly, this work provides support for leveraging the Cu interaction with kinases as a new therapeutic opportunity in targeting aberrantly regulated signaling networks in cancer. To that end, a better understanding of the repertoire of protein kinases that use Cu and the signaling pathways that directly respond to changes in Cu levels will be invaluable to unlocking the therapeutic potential of targeting Cu in not just cancer but many other disease states.

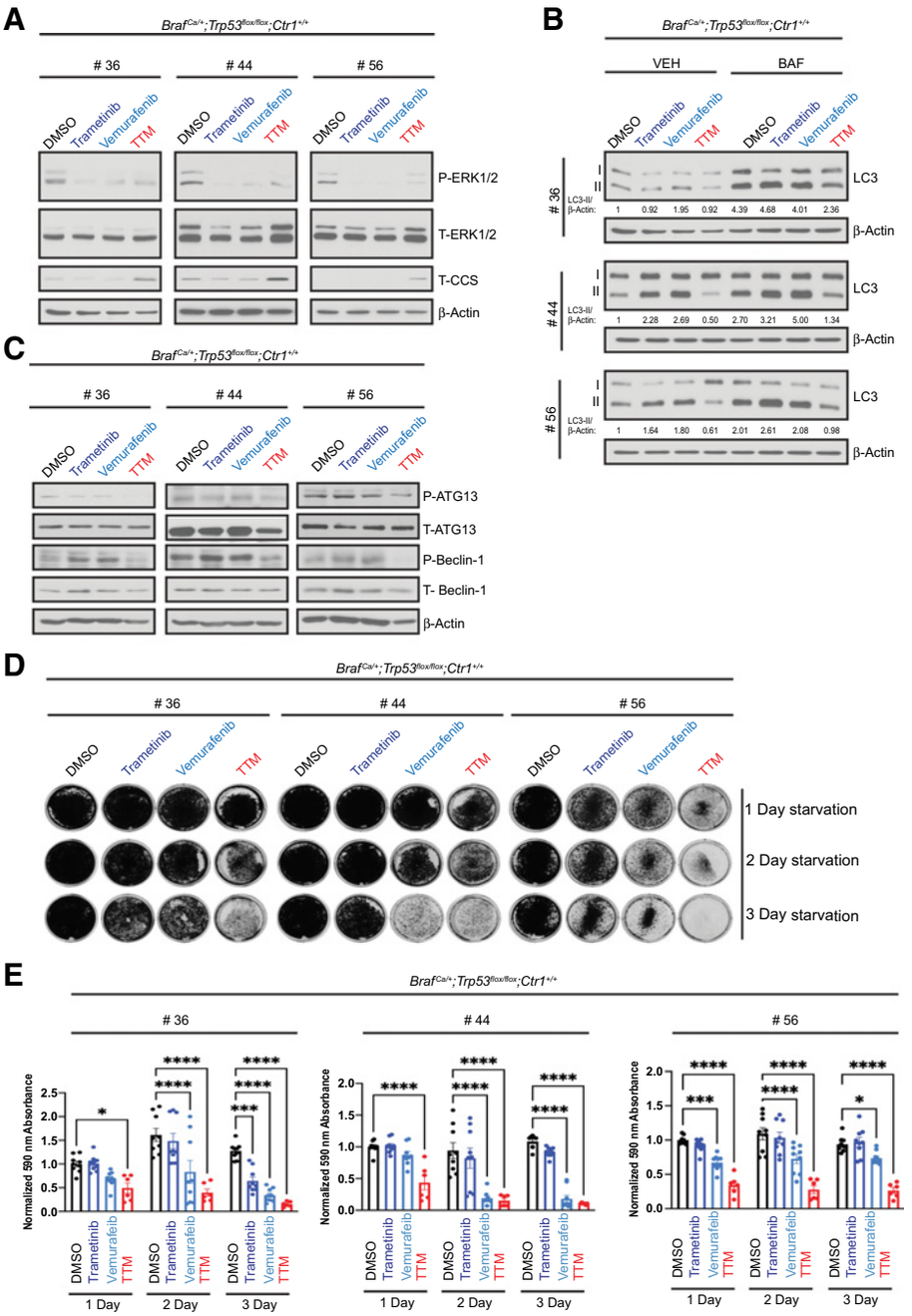

Figure 6.

Cu chelation alters the protective autophagy resulting from MAPK pathway inhibition. **A,** Immunoblot detection of phosphorylated (P) ERK1/2, total (T) ERK1/2, T-CCS, or β-actin from *Braf*$^{CA/+}$;*Trp53*$^{flox/flox}$ (BP) *Ctr1*$^{+/+}$ #36, BP #44, and BP #56 cells treated with DMSO, 1 nmol/L trametinib, 1 μmol/L vemurafenib, or 10 μmol/L tetrathiomolybdate (TTM) for 48 hours. **B,** Immunoblot detection of LC3-I, LC3-II, or β-actin from BP #36, BP #44, and BP #56 cells treated with DMSO, 1 nmol/L trametinib, 1 μmol/L vemurafenib, or 10 μmol/L TTM for 48 hours. Before harvesting, BP cells were treated with vehicle (VEH) or bafilomycin (BAF) for 1 hour. **C,** Immunoblot detection of P-ATG13, T-ATG13, P-Beclin-1, T-Beclin-1, or β-actin from BP *Ctr1*$^{+/+}$ #36, BP #44, and BP #56 cells treated with DMSO, 1 nmol/L trametinib, 1 μmol/L vemurafenib, or 10 μmol/L TTM for 48 hours. **D,** Representative crystal violet images of BP #36, BP #44, and BP #56 cells treated with DMSO, 1 nmol/L trametinib, 1 μmol/L vemurafenib, or 10 μmol/L TTM after 1, 2, or 3 days of starvation followed by recovery in nutrient-replete media. **E,** Scatter dot plot with bar at mean absorbance of extracted crystal violet at 590 nmol/L ± s.e.m. of BP #36, BP #44, and BP #56 cells treated with DMSO, 1 nmol/L trametinib, 1 μmol/L vemurafenib, or 10 μmol/L TTM after 1, 2, or 3 days of starvation followed by recovery in nutrient-replete media normalized to DMSO, 1 day control. Results were compared using a two-way ANOVA followed by Tukey's multi-comparisons test. BP #36, *n* represents number of biologically independent samples; DMSO $n = 9$, Trametinib $n = 9$, Vemurafenib $n = 9$, TTM $n = 6$; *, $P = 0.0234$; ***, $P = 0.0006$; and ****, $P < 0.0001$. BP #44, *n* represents number of biologically independent samples; DMSO $n = 9$, Trametinib $n = 9$, Vemurafenib $n = 9$, TTM $n = 6$; and ****, $P < 0.0001$. BP #56, *n* represents number of biologically independent samples; DMSO $n = 9$, Trametinib $n = 9$, Vemurafenib $n = 9$, TTM $n = 6$; *, $P = 0.0483$; ***, $P = 0.0003$; and ****, $P < 0.0001$.

Authors' Disclosures

T. Tsang reports grants from National Cancer Institute (F31CA243294) and Blavatnik Family Foundation during the conduct of the study. X. Gu reports grants from National Institutes of Health during the conduct of the study. J.M. Posimo reports grants from American Cancer Society during the conduct of the study. D.C. Brady reports grants from National Institutes of Health, Pew Charitable Trust, The V Foundation, and American Cancer Society, other support from University of Pennsylvania Perelman School of Medicine Department of Cancer Biology, and grants from Blavatnik Family Foundation during the conduct of the study; as well as other support from Pleco Therapeutics, Merlon Inc., and Elaeis Therapeutics outside the submitted work; as well as a patent for "Methods of treating and preventing cancer by disrupting the binding of Cu in the MAP kinase pathway (20150017261)" pending. No disclosures were reported by the other authors.

Authors' Contributions

T. Tsang: Conceptualization, data curation, formal analysis, funding acquisition, validation, investigation, visualization, methodology, writing–original draft, writing–review and editing. **X. Gu:** Data curation, formal analysis, validation, investigation, visualization, methodology, writing–review and editing. **C.I. Davis:** Conceptualization, data curation, formal analysis, investigation, visualization, methodology, writing–review and editing. **J.M. Posimo:** Conceptualization, data curation, formal analysis, funding acquisition, investigation, visualization, methodology. **Z.A. Miller:** Data curation, formal analysis, investigation, methodology. **D.C. Brady:** Conceptualization, supervision, funding acquisition, writing–original draft, project administration, writing–review and editing.

Acknowledgments

We thank C.M. Counter, M.S. Crowe, D.G. Kirsch, and D.J. Thiele of Duke University and S.A. Tooze of The Francis Crick Institute for cell lines and mouse models, Martin P. Carroll, E.A. White, J.E. Wilusz, and E.S. Witze (University of Pennsylvania) for technical support, discussions, and/or review of the manuscript, and D. Sneddon for administrative support. This work was supported by NIH grant GM124749, the Pew Charitable Trust Pew Scholars Program in Biomedical Science Award #50359, and The V Foundation Scholar Award 3C59 8ABS 3424 3BDA (to D.C. Brady). T. Tsang is supported by NCI NRSA Fellowship (F31) F31CA243294 and Blavatnik Family Foundation Fellowship. J.M. Posimo is supported by American Cancer Society Postdoctoral Fellowship 131203PF1714701CCG.

The publication costs of this article were defrayed in part by the payment of publication fees. Therefore, and solely to indicate this fact, this article is hereby marked "advertisement" in accordance with 18 USC section 1734.

Note

Supplementary data for this article are available at Molecular Cancer Research Online (http://mcr.aacrjournals.org/).

Received April 5, 2021; revised January 18, 2022; accepted March 17, 2022; published first March 23, 2022.

References

1. Ferguson FM, Gray NS. Kinase inhibitors: the road ahead. Nat Rev Drug Discov 2018;17:353–77.
2. Solomon EI, Heppner DE, Johnston EM, Ginsbach JW, Cirera J, Qayyum M, et al. Copper active sites in biology. Chem Rev 2014;114:3659–853.
3. Turski ML, Brady DC, Kim HJ, Kim BE, Nose Y, Counter CM, et al. A novel role for copper in Ras/mitogen-activated protein kinase signaling. Mol Cell Biol 2012; 32:1284–95.
4. Brady DC, Crowe MS, Turski ML, Hobbs GA, Yao X, Chaikuad A, et al. Copper is required for oncogenic BRAF signalling and tumorigenesis. Nature 2014;509: 492–6.
5. Krishnamoorthy L, Cotruvo JA, Chan J, Kaluarachchi H, Muchenditsi A, Pendyala VS, et al. Copper regulates cyclic–AMP-dependent lipolysis. Nat Chem Biol 2016;12:586–92.
6. Tsang T, Posimo JM, Gudiel AA, Cicchini M, Feldser DM, Brady DC. Copper is an essential regulator of the autophagic kinases ULK1/2 to drive lung adenocarcinoma. Nat Cell Biol 2020;22:412–24.
7. Cotruvo JA, Aron AT, Ramos-Torres KM, Chang CJ. Synthetic fluorescent probes for studying copper in biological systems. Chem Soc Rev 2015;44: 4400–14.
8. Chang CJ. Searching for harmony in transition-metal signaling. Nat Chem Biol 2015;11:744–7.
9. Aron AT, Ramos-Torres KM, Cotruvo JA, Chang CJ. Recognition- and reactivity-based fluorescent probes for studying transition metal signaling in living systems. Acc Chem Res 2015;48:2434–42.
10. Brewer GJ, Johnson V, Dick RD, Kluin KJ, Fink JK, Brunberg JA. Treatment of Wilson disease with ammonium tetrathiomolybdate. Arch Neurol 1996;53:1017.
11. Brady DC, Crowe MS, Greenberg DN, Counter CM. Copper chelation inhibits BRAFV600E-driven melanomagenesis and counters resistance to BRAFV600E and MEK1/2 inhibitors. Cancer Res 2017;77:6240–52.
12. Chan EYW, Kir S, Tooze SA. siRNA screening of the kinome identifies ULK1 as a multidomain modulator of autophagy. J Biol Chem 2007;282: 25464–74.
13. Jung CH, Jun CB, Ro SH, Kim YM, Otto NM, Cao J, et al. ULK–Atg13–FIP200 complexes mediate mTOR signaling to the autophagy machinery. Mol Biol Cell 2009;20:1992–2003.
14. Hosokawa N, Hara T, Kaizuka T, Kishi C, Takamura A, Miura Y, et al. Nutrient-dependent mTORCl association with the ULK1–Atg13–FIP200 complex required for autophagy. Mol Biol Cell 2009;20:1981–91.
15. Russell RC, Tian Y, Yuan H, Park HW, Chang YY, Kim J, et al. ULK1 induces autophagy by phosphorylating Beclin-1 and activating VPS34 lipid kinase. Nat Cell Biol 2013;15:741–50.
16. Polishchuk EV, Merolla A, Lichtmannegger J, Romano A, Indrieri A, Ilyechova EY, et al. Activation of autophagy, observed in liver tissues from patients with Wilson disease and from ATP7B-deficient animals, protects hepatocytes from copper-induced apoptosis. Gastroenterology 2019;156:1173–89.
17. Kinsey CG, Camolotto SA, Boespflug AM, Guillen KP, Foth M, Truong A, et al. Protective autophagy elicited by RAF→MEK→ERK inhibition suggests a treatment strategy for RAS-driven cancers. Nat Med 2019;25:620–7.
18. Bryant KL, Stalnecker CA, Zeitouni D, Klomp JE, Peng S, Tikunov AP, et al. Combination of ERK and autophagy inhibition as a treatment approach for pancreatic cancer. Nat Med 2019;25:628–40.
19. Lee CS, Lee LC, Yuan TL, Chakka S, Fellmann C, Lowe SW, et al. MAP kinase and autophagy pathways cooperate to maintain RAS mutant cancer cell survival. Proc Natl Acad Sci U S A 2019;116:4508–17.
20. Guo JY, Karsli-Uzunbas G, Mathew R, Aisner SC, Kamphorst JJ, Strohecker AM, et al. Autophagy suppresses progression of K-ras-induced lung tumors to oncocytomas and maintains lipid homeostasis. Genes Dev 2013; 27:1447–61.
21. Strohecker AM, Guo JY, Karsli-Uzunbas G, Price SM, Chen GJ, Mathew R, et al. Autophagy sustains mitochondrial glutamine metabolism and growth of BrafV600E-driven lung tumors. Cancer Discov 2013;3:1272–85.
22. Marchetti A, Felicioni L, Malatesta S, Sciarrotta MG, Guetti L, Chella A, et al. Clinical features and outcome of patients with non–small cell lung cancer harboring BRAF mutations. J Clin Oncol 2011;29:3574–9.
23. Mazieres J, Cropet C, Montané L, Barlesi F, Souquet PJ, Quantin X, et al. Vemurafenib in non–small cell lung cancer patients with BRAFV600 and BRAFnonV600 mutations. Ann Oncol 2020;31:289–94.
24. Planchard D, Smit EF, Groen HJM, Mazieres J, Besse B, Helland Å, et al. Dabrafenib plus trametinib in patients with previously untreated BRAFV600E-mutant metastatic non–small cell lung cancer: an open-label, phase 2 trial. Lancet Oncol 2017;18:1307–16.
25. McAlpine F, Williamson LE, Tooze SA, Chan EYW. Regulation of nutrient-sensitive autophagy by uncoordinated 51-like kinases 1 and 2. Autophagy 2013;9: 361–73.
26. N'Diaye EN, Kajihara KK, Hsieh I, Morisaki H, Debnath J, Brown EJ. PLIC proteins or ubiquilins regulate autophagy-dependent cell survival during nutrient starvation. EMBO Rep 2009;10:173–9.
27. Sanjana NE, Shalem O, Zhang F. Improved vectors and genome-wide libraries for CRISPR screening. Nat Methods 2014;11:783–4.
28. Li X, Newbern JM, Wu Y, Morgan-Smith M, Zhong J, Charron J, et al. MEK is a key regulator of gliogenesis in the developing brain. Neuron 2012;75: 1035–50.

29. Gillingham AK, Bertram J, Begum F, Munro S. In vivo identification of GTPase interactors by mitochondrial relocalization and proximity biotinylation. Elife 2019;8:e45916.
30. Hamad NM, Elconin JH, Karnoub AE, Bai W, Rich JN, Abraham RT, et al. Distinct requirements for Ras oncogenesis in human versus mouse cells. Genes Dev 2002;16:2045–57.
31. Nose Y, Kim B-E, Thiele DJ. Ctr1 drives intestinal copper absorption and is essential for growth, iron metabolism, and neonatal cardiac function. Cell Metab 2006;4:235–44.
32. Dankort D, Filenova E, Collado M, Serrano M, Jones K, McMahon M. A new mouse model to explore the initiation, progression, and therapy of BRAFV600E-induced lung tumors. Genes Dev 2007;21:379–84.
33. Brady GF, Galbán S, Liu X, Basrur V, Gitlin JD, Elenitoba-Johnson KSJ, et al. Regulation of the copper chaperone CCS by XIAP-mediated ubiquitination. Mol Cell Biol 2010;30:1923–36.
34. Ganley IG, Lam DH, Wang J, Ding X, Chen S, Jiang X. ULK1·ATG13·FIP200 complex mediates mTOR signaling and is essential for autophagy. J Biol Chem 2009;284:12297–305.
35. Park JM, Seo M, Jung CH, Grunwald D, Stone M, Otto NM, et al. ULK1 phosphorylates Ser30 of BECN1 in association with ATG14 to stimulate autophagy induction. Autophagy 2018;14:584–97.
36. Ichimura Y, Kirisako T, Takao T, Satomi Y, Shimonishi Y, Ishihara N, et al. A ubiquitin-like system mediates protein lipidation. Nature 2000;408:488–92.
37. Itoh T, Fujita N, Kanno E, Yamamoto A, Yoshimori T, Fukuda M. Golgi-resident small GTPase Rab33B interacts with Atg16L and modulates autophagosome formation. Mol Biol Cell 2008;19:2916–25.
38. Kim DH, Sarbassov DD, Ali SM, King JE, Latek RR, Erdjument-Bromage H, et al. mTOR interacts with raptor to form a nutrient-sensitive complex that signals to the cell growth machinery. Cell 2002;110:163–75.
39. Amaravadi RK, Kimmelman AC, Debnath J. Targeting autophagy in cancer: recent advances and future directions. Cancer Discov 2019;9:1167–81.
40. Costedoat-Chalumeau N, Hulot JS, Amoura Z, Delcourt A, Maisonobe T, Dorent R, et al. Cardiomyopathy related to antimalarial therapy with illustrative case report. Cardiology 2007;107:73–80.
41. Melles RB, Marmor MF. The risk of toxic retinopathy in patients on long-term hydroxychloroquine therapy. JAMA Ophthalmol 2014;132:1453–60.
42. Pellegrini P, Strambi A, Zipoli C, Hägg-Olofsson M, Buoncervello M, Linder S, et al. Acidic extracellular pH neutralizes the autophagy-inhibiting activity of chloroquine: implications for cancer therapies. Autophagy 2014;10:562–71.
43. Ala A, Walker AP, Ashkan K, Dooley JS. Wilson's disease. Lancet 2007;369:397–408.
44. Chan N, Willis A, Kornhauser N, Mward M, Lee SB, Nackos E, et al. Influencing the tumor microenvironment: a Phase II study of copper depletion using tetrathiomolybdate in patients with breast cancer at high risk for recurrence and in preclinical models of lung metastases. Clin Cancer Res 2017;23:666–76.